Phase space approach for modeling of epileptic dynamics

Yujiang Wang,[1,*] Marc Goodfellow,[2] Peter Neal Taylor,[1] and Gerold Baier[1]
[1]*Doctoral Training Centre Integrative Systems Biology, Manchester Interdisciplinary Biocentre, 131 Princess Street, Manchester M1 7DN, United Kingdom*
[2]*Centre for Interdisciplinary Computational and Dynamical Analysis (CICADA), Alan Turing Building, Manchester M13 9PL, United Kingdom*
(Received 14 February 2012; revised manuscript received 13 May 2012; published 22 June 2012)

Epileptic electroencephalography recordings can be described in terms of four prototypic wave forms: fast sinusoidal oscillations, large slow waves, fast spiking, and spike waves. On the macroscopic level, these wave forms have been modeled by different mechanistic models which share canonical features. Here we derive a minimal model of excitatory and inhibitory processes with features common to all previous models. We can infer that at least three interacting processes are required to support the prototypic epileptic dynamics. Based on a separation of time scales we analyze the model in terms of interacting manifolds in phase space. This allows qualitative reverse engineering of all epileptic wave forms and transitions between them. We propose this method as a complement to traditional approaches to modeling epileptiform rhythms.

DOI: 10.1103/PhysRevE.85.061918 PACS number(s): 87.19.xm, 87.19.le, 05.45.−a

I. INTRODUCTION

Epileptic seizures are accompanied by a large variety of wave forms in the electroencephalogram (EEG). Despite their differences, detailed studies have characterized a small number of typical wave forms that recur in clinical recordings [1,2]. These wave forms are

(a) sinusoidal waves of low amplitude, which can vary greatly in frequency; Vary w/ time, person to person, or what?

(b) spikes with a distinct anharmonic wave form which are higher in amplitude than the sinusoidal oscillations (if their frequency is less than 14 Hz they are referred to as "sharp waves");

(c) high-amplitude slow waves, which are under 8 Hz, without a distinct peak in the wave form;

(d) spike waves, which are similar in amplitude and frequency to the slow waves, but have single or multiple spikes (or sharp waves) interspersed between the waves.

Additionally, in Ref. [2] the possibility of transitions between these wave forms during a single seizure is emphasized, i.e., a seizure can be composed of segments with different prototypic wave forms. Therefore, a small number of common EEG wave forms are used to describe a large number of epileptic seizure types [3]. This might suggest that some unifying principles underlie the generation of the epileptic EEG, although the actual (neurophysiological) causes leading to the generation of these rhythms might be very different. Therefore a unifying framework for a comprehensive explanation of macroscopic epileptic dynamics should be able to capture the aforementioned types of wave form.

It is generally believed that excitatory and inhibitory processes in the brain are important for epileptic EEG wave forms [4]. One approach to describe EEG dynamics is therefore to assume a number of populations of neurons and their excitatory and inhibitory interactions on the macroscopic scale (see [5,6] for reviews and references therein). These models (e.g., [7–14]) are termed neural mass or neural field models, or lumped models. They generally assume that low-dimensional attractors underlie the epileptiform EEG recordings and they are used to make inferences about potential mechanisms of specific epileptic seizures.

There are a number of tools to analyze the dynamics of these model equations. Arguably the most popular technique is parameter sampling or bifurcation scanning (direct or continuation). However, thorough bifurcation analysis of these systems of coupled nonlinear differential equations is feasible in only a few of the model parameters (typically between one and three). As the presented modeling results rely on specific fixed values of parameters other than those studied, this implies that these are assumed to be correct. In reality, different patients with the same type of seizure will have different global parameter settings, and even within one patient the parameters may change dramatically, e.g., during brain development in childhood. In addition, few if any of the parameter values are rigorously determined by physiological measurement or can directly be related to experimental data. Hence the exact global parameter setting is rarely known. In the general (neuroscience) modeling literature, systematic studies of multiple parameters have been suggested by parameter space sampling and investigating the variance of the output [15], or by the so-called "metabifurcation" analysis [16]. However, these studies are time consuming, demand high computational power, and are currently not done routinely for neural mass modeling studies of epilepsy.

A complementary approach is to characterize the (minimal) conditions or model assumptions required to generate epileptiform rhythms. If the assumption of epileptic rhythms being low-dimensional attractors [17] is correct, then they can in principle be reverse engineered in a low-dimensional phase space. Steps in this direction were suggested in Ref. [18] for systems with separable slow-fast time scales. The main idea is to understand the system in terms of modular structures in phase space. Such an approach has, to our knowledge, not been used to explain prototypic epileptic behavior on the neural mass level. Furthermore, the author of Ref. [19] has shown that such an approach can lead to a general classification of the system in terms of normal forms, or prototypes, which

*yujiang.wang-2@postgrad.manchester.ac.uk

in our case correspond to prototypic epileptiform behavior. A recent study has suggested a similar idea (a dictionary of mappings between behavior of the system and certain patterns of observed activity) for epileptic EEG rhythms. Moreover, this study explicitly calls for a " 'minimal model' that can economically account for all these behaviors" [20].

Here, we propose a minimal neural mass model framework that is able to generate epileptic wave forms in terms of interacting excitatory and inhibitory neural processes. We show that the time scale separation in the system can be used to understand the phase space structures and to classify prototypes of epileptiform dynamics. Furthermore we use this knowledge to reverse engineer a variety of other relevant epileptic phenomena.

II. THE MINIMAL NEURAL MASS MODEL

Three main assumptions form the basis of this modeling approach. First, epileptic EEG dynamics can be understood on the macroscopic level in terms of interacting excitatory and inhibitory processes [4]. Second, we assume that the prototypical epileptic rhythms are explained by low-dimensional attractors [8]. Third, according to the neural mass modeling literature, the main factors which determine the dynamics are the feedback structure, the coupling via sigmoidal activation, and the characteristic time scales [6,21,22].

The single-location Wilson-Cowan system [21] is one of the best-studied population level model systems (see, for example, [21,23–25]) that incorporates all these main factors. We base our minimal model on the Wilson-Cowan formalism and include a second slow inhibitory process which is motivated by consistent experimental and modeling findings within the context of epileptic dynamics that inhibitory processes are assumed to work on two different time scales [7,26]. The inclusion of a second inhibitory population is also in agreement with recent neural mass modeling assumptions [12,14], and we will show in the presentation of the results that the inclusion is required to reconstruct prototypical dynamics.

The general system of three coupled processes is

$$\begin{aligned}\tau_x \frac{dx}{dt} &= -x + S(C_{x,x}x + C_{x,y}y + C_{x,z}z + P),\\ \tau_y \frac{dy}{dt} &= -y + S(C_{y,x}x + C_{y,y}y + C_{y,z}z + Q),\\ \tau_z \frac{dz}{dt} &= -z + S(C_{z,x}x + C_{z,y}y + C_{z,z}z + R).\end{aligned} \tag{1}$$

Here, x represents an excitatory process, and y and z represent inhibitory processes. Each equation has a linear term leading to exponential decay in the absence of any other input. Input from neural processes or from the environment is passed through an activation function $S(\cdot)$. The connectivity constants $C_{i,j}$ $(i,j = x,y,z)$ determine the strength of coupling from the j variable to the rate equation of the i variable. $C_{i,y}$ and $C_{i,z}$ are negative (or zero) and $C_{i,x}$ are positive (or zero) for all i. The x,y subsystem (when $C_{x,z} = C_{y,z} = 0$) is the previously studied Wilson-Cowan oscillator. In the following we also refer to this two-variable oscillator as the (Wilson-Cowan) *subsystem* and refer to the three-variable system as the *full system*. External inputs are modeled by constants P, Q, and R, which can also be interpreted as the general excitability level, as they determine how much input is required to activate a process.

We now consider the individual components of the model separately to account for their role in the bifurcation behavior of the subsystem.

Feedback structure. We first describe the effect of the feedback structure in the subsystem with $\tau_x = \tau_y$. As an unstable focus is of particular interest for the following analysis, we derive the minimal feedback structure, based on the eigenvalues in a linear system [see Appendix A and Eq. (A2)], to be self-excitation of the excitatory populations and mutual activation of the two processes. The frequency in the vicinity of the focus increases both with increasing $C_{y,x}$ and with increasing $|C_{x,y}|$ (see Appendix A). These properties are preserved locally, when using a sigmoid as the activation function.

Sigmoidal activation. Using the sigmoidal activation as in the original Wilson-Cowan system, the function $S(\cdot)$ in the subsystem becomes $S(\chi) = \frac{1}{1+\exp[-a(\chi-\theta)]}$. Unless otherwise stated, we set the steepness of the sigmoid to $a = 1$ and the threshold to $\theta = 4$. Fixing these specific values is justified, as scaling all the values of the connectivities and the inputs will have the same effect as changing the steepness (a) of the sigmoid and changing the inputs will have the same effect as changing the offset (θ) of the sigmoid.

The nullclines of the subsystem with sigmoidal activation are $\frac{dx}{dt} = 0 \Rightarrow y = \frac{\frac{\ln(1/x-1)}{-a}+\theta-P-C_{x,x}x}{C_{x,y}}$ and $\frac{dy}{dt} = 0 \Rightarrow x = \frac{\frac{\ln(1/y-1)}{-a}+\theta-Q-C_{y,y}y}{C_{y,x}}$. Depending on the position of the nullclines, the subsystem can have two saddle-node pairs and a focus. Their existence can be verified and their number and position can be controlled with the connectivity parameters and the inputs (but not the time scale parameters). For the case of an unstable focus, analytical conditions for the existence of a limit cycle in the Wilson-Cowan subsystem are given in Ref. [25].

Time scale parameters. A difference in time scales of the subsystem does not alter the shape or position of the nullclines. However, it changes the relative magnitude of the vector field (defined by the differential equation) in the respective directions. Thus the time scale parameters can affect the eigenvalues of the focus, and it can be shown that increase of the ratio $\frac{\tau_x}{\tau_y}$ increases the frequency of the limit cycle and decreases its amplitude (see Appendix A). This can shift and therefore control the homoclinic bifurcation, the saddle-node on invariant circle and the Hopf bifurcation points of the system.

Bifurcations in the subsystem. The coupling of a third variable to x corresponds to a time-dependent modulation of the parameter P. To understand the impact of an additional slow process z we can therefore first consider changes in phase space structure for different P. This has been studied extensively in previous work (for example, [24]). We summarize these results and present them in a light that will facilitate the understanding of our results.

Figure 1 shows four exemplary bifurcation diagrams of the Wilson-Cowan subsystem, which will be used in the Results section. As shown, it is possible to fully control the bifurcations of the fixed points. Additionally the limit

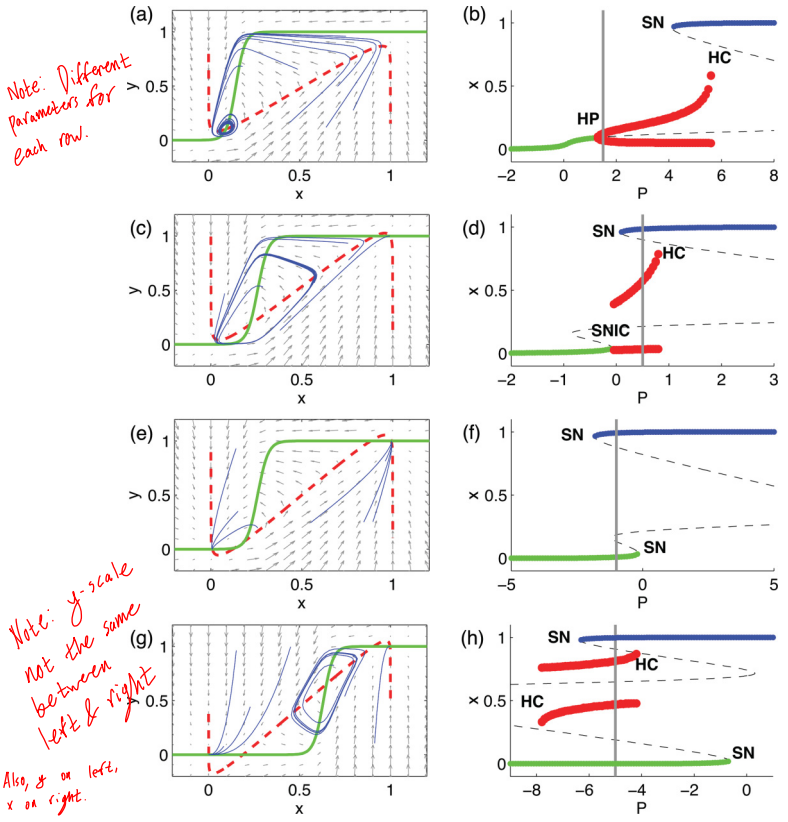

FIG. 1. (Color online) Left: Phase space plots of the subsystem showing the x nullcline [dashed thick (red) line], the y nullcline [solid thick (green) line], trajectories from random initial conditions [solid thin (blue) lines], and the vector field (gray arrows). Right: Bifurcation diagrams of the subsystem for P showing the x values of the fixed points [small (green or blue) markers], or the maxima and minima of the limit cycle [big (red) markers]. Gray thin dashed line, unstable fixed points; HP, Hopf bifurcation; HC, homoclinic bifurcation; SN, saddle-node bifurcation; SNIC, saddle node on invariant circle bifurcation; thick gray vertical line, the value of P used in the corresponding phase space (left). The parameters are given in Appendix B.

cycle can be controlled with the time scale parameters. Therefore, the three stable structures (upper and lower fixed points and the limit cycle) can be understood as separate modules that determine the dynamics of the Wilson-Cowan subsystem.

Addition of a slow inhibitory process. In order to account for more complex dynamics such as spike waves or polyspike waves, an at least three-dimensional ordinary differential equation (ODE) system is required, as the two-dimensional system can have only a simple limit cycle or fixed points, as shown in the previous analysis and in Refs. [19,25]. We introduce a slow inhibitory process following [14] and get to the full system as defined in Eq. (1). The nullcline plane defined by the condition $\frac{dz}{dt} = 0$ is given by the following equation:

$$\frac{dz}{dt} = 0 \Rightarrow z = \frac{1}{1 + \exp[-a(C_{z,x}x + C_{z,y}y + C_{z,z}z + R - \theta)]}. \quad (2)$$

III. RESULTS

A. Phase space of the minimal model

In order to model more complex dynamics, including the prototypical spike-wave dynamics, we use the full three-dimensional system with $\tau_x \approx \tau_y \ll \tau_z$. In the limit of constant values of z (the speed of z is infinitely slow; $\forall t, \frac{dz}{dt} = 0$) the invariant structures of the Wilson-Cowan subsystem (saddles, nodes, and limit cycles) form a manifold in the full, three-dimensional phase space, termed the "critical manifold." Figure 2 shows the resulting phase space picture for this limit. The structures are in essence the bifurcation scan in Fig. 1(a), but shown in three dimensions.

When the speed of z is not infinitely slow, Fenichel's theorem [27] states the existence of slow manifolds (Fenichel manifolds) close to the critical manifolds in the phase space of the full system. In that case, the time scale separation determines how close the Fenichel manifolds are to the critical manifolds [27].

In addition to the critical manifold, the $\frac{dz}{dt} = 0$ nullcline plane [see Eq. (2)] is calculated for the full phase space. The nullcline plane divides the phase space into two subspaces. Above the plane (in the positive z direction) the flow of the vector field in phase space is in the negative z direction, and vice versa. Therefore, the nullcline plane is attractive in the z direction, and the further away from the plane, the stronger the flow in the z direction. We consider the simplest case, when z receives only positive input from x and is coupled only negatively to x ($C_{z,y} = C_{z,z} = 0$, $C_{z,x} > 0$, and $C_{x,z} < 0$). The nullcline plane Eq. (2) simplifies to $z = \frac{1}{1+\exp[-a(C_{z,x}x+R-\theta)]}$. Therefore, $C_{z,x}$ scales the nullcline plane and the input parameter R shifts the plane in the negative x direction. The time scale parameter τ_z determines how fast trajectories are attracted to the $\frac{dz}{dt}$ nullcline plane in the direction of z.

The intersections of this nullcline plane with the critical fixed point manifolds are the fixed points of the full system. In general, the intersections of Fenichel manifolds and the

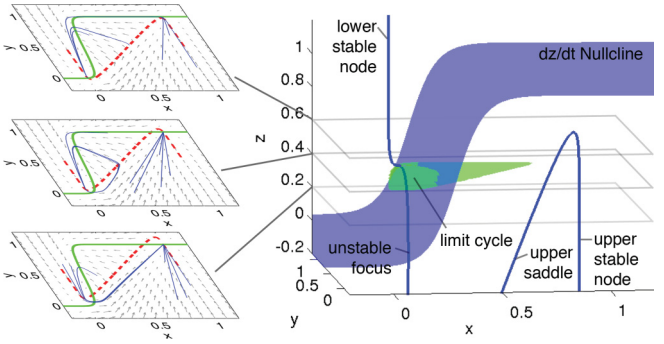

FIG. 2. (Color online) Right: Phase space of the full system [Eq. (1)] with the critical fixed point manifold [solid (blue) line], the critical limit cycle manifold [conelike (green) surface], and the $dz/dt = 0$ nullcline plane [S-shaped (blue) surface]. Left: Three exemplary phase planes of the subsystem are shown for constant z values indicated by the cross section in the full phase space. Refer to Fig. 1 for the subsystem phase space plotting convention. The parameters are given in Appendix B. The three-dimensional (3D) plot can be found in the Supplemental Material [28].

nullcline plane stabilize attractors that are locally similar to the corresponding attractors of the critical manifold.

Following [8] we consider the epileptic rhythms to be generated by limit cycle attractors in the minimal model. In the following, we use the critical manifolds as an approximation to the Fenichel manifolds for visualization and reconstruct the dynamics of prototypic wave forms as limit cycles in the full system.

In detail, the steps that have to be followed to reconstruct observed wave forms are (i) determine the subsystem structure(s) required; (ii) determine how the subsystem structures need to be arranged relative to each other, such that the flow in the three-dimensional phase space can connect them; (iii) reconstruct the subsystem bifurcation diagram for P from (ii); (iv) organize the nullcline plane such that it directs the flow in the full system as desired. These steps will be followed for the reconstruction of the prototypical wave forms.

B. Prototypes of epileptic wave forms

Sinusoidal waves. Figure 3(b) shows an example of fast (≈20 Hz) sinusoidal oscillations from an EEG recording of a 1.5-year-old male with focal epilepsy. The fast oscillation appears from an irregular background, is low in amplitude (compared to other epileptic rhythms), and in this case precedes irregular seizure activity. Such fast activity is often observed near the onset of focal seizures [2].

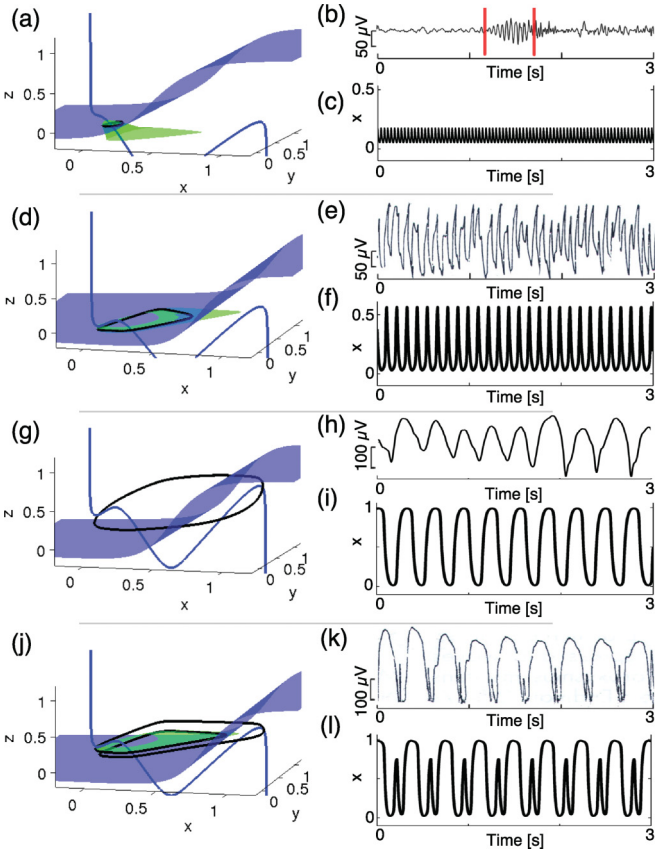

FIG. 3. (Color online) Left: Full phase space reconstructions of prototypes, where the attractor is plotted with a thick black line. Refer to Fig. 2 for the plotting convention. Right: Corresponding exemplary EEG and model time series. In (b) only the region between the markers (red) is the sinusoidal wave form. The x variable is used as model output. EEGs in (e) and (k) are reproduced and modified with permission from Ref. ([29], pp. 279 and 152). The parameter values are given in Appendix B. The 3D plots are in the Supplemental Material [28].

The two-dimensional Wilson-Cowan subsystem can display sinusoidal oscillations, due to the existence of a limit cycle from a Hopf bifurcation [21,24] [Fig. 1(b)]. In order to preserve this limit cycle in the full system, the $\frac{dz}{dt}$ sigmoid-shaped nullcline plane needs to intersect the limit cycle manifold, for instance its lower part. In the vicinity of this intersection, the flow in the z direction is almost zero, and the only dominant dynamic is the oscillation of the limit cycle [see Figs. 3(a) and 3(c)].

Spike trains. Figure 3(e) shows an EEG from a 12-year-old male with Lennox-Gastaut syndrome in a tonic seizure ([29], p. 279). The EEG is dominated by spikes. Relative to the background, the spike is higher in amplitude than the sinusoidal oscillations and the frequency in this case is around 11 Hz.

To reconstruct the spike attractor, we start with the knowledge that the subsystem can display spiking dynamics in a limit cycle near a homoclinic bifurcation. To preserve the spike limit cycle in the full system, we intersect the limit cycle manifold near the homoclinic bifurcation with the nullcline plane [see Fig. 1(d) for the subsystem bifurcation, Fig. 3(d) for the configuration of the full system, and Fig. 3(f) for the time series].

Note that both the sinusoidal oscillations and the spike trains can be found in the two-dimensional fast subsystem already. The next two wave forms (specifically the spike-wave form) require the addition of an additional slow variable.

Slow waves. The slow wave is a high-amplitude oscillation below 8 Hz. It is called "slow" relative to the above sinusoidal oscillations and spikes. This wave form usually does not have a sharp peak. Figure 3(h) shows an example EEG from a 12-year-old female during the final part of a focal-onset seizure.

The structures that can be used to model slow waves are the two fixed point Fenichel manifolds when they coexist for a certain range of z [or P, as in the central part of Fig. 1(f)]. In this case, the subsystem does not need to have a limit cycle manifold. The nullcline plane separates the upper fixed point from the lower fixed point manifolds such that they are both unstable in the full system in opposite z directions [Fig. 3(g)]. This configuration then gives rise to the slow wave oscillations by autonomously switching from one fixed point manifold to the other [Fig. 3(i)]. The exact frequency depends crucially on the choice of the slow time scale parameter τ_z.

Spike waves. The spike-wave form is typical for generalized seizures, and Fig. 3(k) shows a section of an EEG trace of a 10-year-old female during a typical absence seizure, where a single spike separates large-amplitude slow waves ([29], p. 152, Fig. 143).

To construct the spike-wave wave form, the bistability of the upper fixed point (wave component) and the limit cycle (spike component) in the subsytem [Fig. 1(d)] is crucial. Used in the full system with a nullcline plane that separates the two structures, will enable autonomous switching between the two structures, as for the wave attractor [Fig. 3(j)]. The resulting wave form then combines the features of slow waves and spikes [Fig. 3(l)].

The single-spike-wave form is a special case of the polyspike-wave form, which is also found clinically. It can be reconstructed starting from the single-spike-wave case. The velocity of the trajectory on the limit cycle manifold determines the number of spikes between the waves. In essence the length of the limit cycle manifold in the z direction and τ_z are the parameters controlling the number of spikes between the wave. In fact, τ_z can be estimated depending on how many spikes are required in the polyspike wave, as demonstrated in the context of mixed mode oscillations in Ref. [18].

The described prototypic wave forms can be used as classifiers of the system, as the prototypes correspond to simple states of the system in terms of global stability of the Fenichel manifolds (or as an approximation, critical manifolds). A globally stable fixed point, which corresponds to an intersection of the stable fixed point manifold with the nullcline plane is the first class of attractors. The second class of attractors are simple limit cycles [spikes and sinusoidal oscillations; see Figs. 3(a) and 3(d)]. Here the limit cycle manifold of the fast subsystem is stabilized globally. For the wave prototype class [Fig. 3(g)], the two stable fixed point manifolds coexist for certain values of z and they are globally unstable in the full system in opposite z directions. For the spike-wave class [Fig. 3(j)] the fixed point manifolds as well as the limit cycle manifold are unstable in the full system in opposite z directions. Symmetric cases exist for the classes of the attractors. These symmetric wave forms reverse the role of the upper and lower saddle and fixed points in the subsystem such that the time series appears upside down.

I need to download the code/ figures from the SE.

C. Parameter-induced transitions

Epileptic seizure EEG recordings often show the transition of one prototypic wave form to another. With our approach, it can be suggested how the phase space components have to change relative to each other to output the observed transitions. From this, it can be hypothesized which potential parameter changes underlie the transition.

In the following we apply this approach to examples of relevance in epilepsy research. Figure 4(a) shows an EEG recording of a seizure in a pediatric patient with myoclonic epilepsy as an example of a transition from spiking dynamics to polyspike-wave dynamics. We model this by using the property that the (spike) limit cycle manifold is stable only if the intersection with the nullcline plane in the central part keeps the flows up- and downward on either side of the plane in balance [Fig. 4(b)]. If this is not the case the spike limit cycle is destabilized and, if the configurations of other components allow it, the polyspike-wave attractor can appear [Fig. 4(c)]. Figure 4(d) shows a simulation, where following the selection of the described phase space structure for spiking, the input parameter P is slowly increased to model the abrupt transition from spike-wave to polyspike-wave dynamics.

A more subtle example is the often observed frequency slowing during absence seizures from about 3 to 2.5 Hz or less [30], which typically manifests in longer-wave components towards the end of the seizure. In terms of phase space configuration this means that the trajectory remains longer on the slow manifold of the upper fixed point. This can be achieved either by changing the degree of attraction of the nullcline plane (changing τ_z) or by moving the nullcline plane closer to the upper saddle-node manifold in the z direction to decrease the strength of the upward flow. In Fig. 5, $C_{z,x}$ has been changed gradually to follow the latter approach [as shown in Figs. 5(b)—before the change, and 5(c)—after

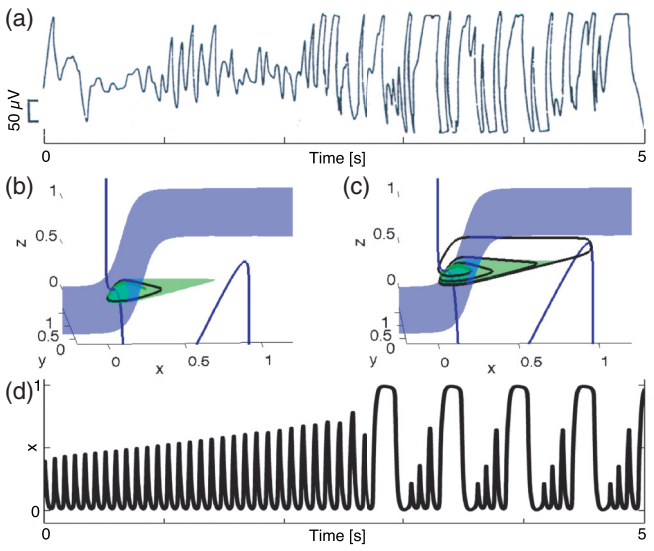

FIG. 4. (Color online) (a) Transition of epileptic wave forms in clinical EEG from spike to polyspike wave. (Reproduced and modified with permission from Ref. ([29], p. 279).) (b),(c) Corresponding phase space structures for spiking and polyspike waves. Refer to Fig. 2 for the plotting convention of phase space. (d) x time course as P is increased gradually from the setting in (b) to (c). The parameters are given in Appendix B. The 3D plots are in the Supplemental Material [28].

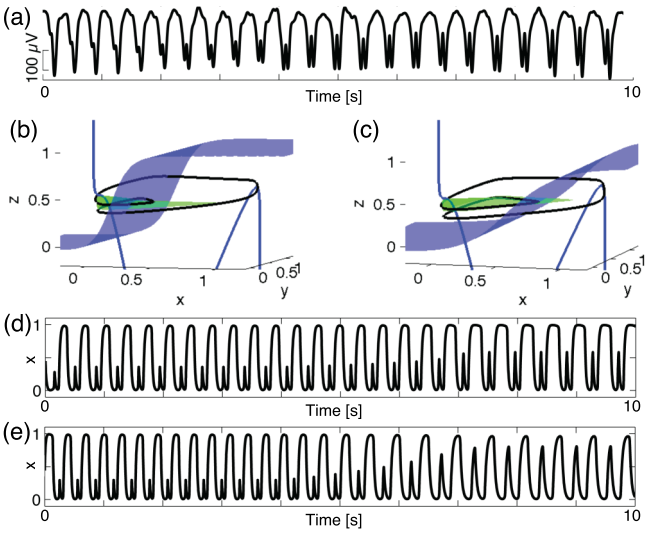

FIG. 5. (Color online) (a) Clinical EEG recording of an absence seizure with slowing of frequency. (b),(c) Phase space configurations at the beginning and the end of the time series in (d). Refer to Fig. 2 for the plotting convention of phase space. (d) Time series of variable x as parameter $C_{z,x}$ is gradually varied. (e) Time series of variable x as parameters τ_x and τ_y are gradually varied. See Table I in Appendix B for details. The 3D plots are in the Supplemental Material [28].

the change]. In contrast, Fig. 5(e) shows one possibility to induce frequency slowing by slowing down the subsystem (x and y were changed to about one-half of their original speed). In this case particularly the spike becomes broader. According to the wave form output, this resulting wave form does not agree with the EEG observations. This demonstrates that bifurcation scans of simple properties in the time series are often not enough to detect certain types of behavior. In contrast, the mechanistic (dynamical) understanding of the system in this case enables us to reconstruct the exact observation and formulate hypotheses on the underlying parameter changes of certain observations.

What's the actual biochemical/neurological meaning of the parameters though?

In addition to parameter-dependent attractor dynamics, excitability (epileptiform wave forms induced by perturbations) and bistability (the coexistence of normal and epileptic attractors) can be reconstructed in the current framework. This is shown in Appendix C with the example of interictal spikes (Fig. 7) and the bistability between a fixed point and a spike-wave attractor (Fig. 8). The impact of noisy input parameters and the conditions for the robustness of the attractors against additive noise are demonstrated in Appendix D.

IV. DISCUSSION

In this work we presented a minimal system of three generic neural processes to model prototypic epileptic rhythms. Rhythms were composed in a modular way from basic phase space structures of the system. This approach enables reverse engineering of epileptic EEG phenomena.

The four prototypes of epileptic seizure rhythms were reconstructed as periodic attractors. These prototypes can be used to classify the configuration of the system. In this sense, we follow the (dynamic) "dictionary" idea from [20]. Additionally, we have now shown that a minimal model approach is possible (based on generic mass modeling assumptions), and our analysis goes beyond the suggested dictionary mapping as we demonstrate how epileptic prototypes can be reverse engineered.

Fast sinusoidal waves arise from a supercritical Hopf bifurcation of the focus. Such a Hopf oscillation has previously been used to account for fast oscillations at the onset of focal epileptic seizures in a neural mass modeling context [11]. Additionally, it was suggested that a noise-driven focus near the Hopf bifurcation could account for similar types of sinusoidal oscillations [20]. In our model, it is possible to flexibly adjust the frequency of the oscillation with the model parameters, as the dependency of the parameters is analytically known. We can thereby account for the clinically observed variability of the frequency in this type of oscillation. One concern in the context of high-frequency oscillations is that the Wilson-Cowan equations hold only for slowly changing dynamics as they are derived under the assumption of temporal coarse graining. However, a recent study demonstrated that the Wilson-Cowan description can be used as an approximation for population oscillation frequencies up to the γ range (30–100 + Hz) [31].

Spike trains were modeled near the homoclinic bifurcation of the limit cycle in the Wilson-Cowan subsystem. However, other bifurcations are possible, notably saddle-node bifurcation on invariant circle. This is in line with studies in Refs. [7,20] where limit cycles near these two bifurcations were used to model epileptic rhythms with large amplitudes and anharmonic wave forms.

Slow waves were reconstructed using the slow manifolds of two stable nodes in the full system to account for both their large amplitude and their low frequency. This agrees with similar observations in systems which also contain two distinct inhibitory processes at two different time scales [7].

The spike-wave attractor is of particular relevance for generalized [1] and focal [2] seizure dynamics. Following a previous suggestion [14], we described it as a type of bursting dynamics.[1] In fast-slow systems with three variables, all possible bursting configurations were classified in Ref. [19]. Adopting that classification for our macroscopic model, the specific spike-wave prototype [Fig. 3(j)] used in this work falls under the case of "fold/homoclinic bursting" however, more complicated situations, e.g., "Hopf/homoclinic bursting" can also be used in the current model.

EEG recordings of epileptic seizures can be a mixture of different prototypes. For example, in Ref. [2] some typical evolutions of partial seizures were characterized. We demonstrated that such transitions can be understood as morphing phase space configurations corresponding to different prototypes into one another. This is in line with the concept of a "dynamical disease" as discussed in Ref. [32], where it was proposed that changes from one type of pathological dynamics to another can be due to bifurcations occurring during slow changes of critical parameters. The example shown here (Fig. 4) used variation of a single parameter. In general, multiple model parameter changes can be involved in the explanation of a given phenomenon [33].

Reverse engineering of the typical frequency slowing in absence seizures (Fig. 5) demonstrates that the model might allow for a number of options to explain additional, more specific observations. Interestingly, although the frequency slowing of spike-wave dynamics is a characteristic feature in typical absence seizures, previous neural mass modeling approaches [9,12,26,34] have not studied it so far.

The reverse-engineering process shown here is not automated and requires a human operator to understand the bifurcations of the subsystem and reconstruct the Fenichel manifolds in the full system. However, one could imagine an automation of the process in parts by following the steps in Sec. III A to facilitate the application of this approach. The important and significant advantage of this approach in the context of epileptic attractors is the mechanistic understanding and classification of the system, which enables reconstruction of attractors. The usefulness and strength of such an approach has been demonstrated in Ref. [19] in a different area of research.

The application of this methodology to other nonminimal models of epileptic dynamics or of general brain dynamics with possibly higher dimensions is nontrivial. However, it is demonstrated in Ref. [18] that other systems with different fast-slow configurations can still be theoretically analyzed. Naturally, as the dimensionality of the analyzed system

[1]Note that "bursting" here does not refer to *neuronal* bursting but to population level dynamics.

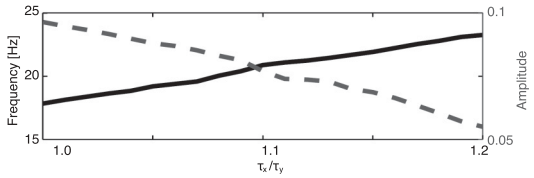

FIG. 6. Scan of the frequency (solid black line) and amplitude (gray dashed line) of the limit cycle in the smooth sigmoidal Wilson-Cowan subsystem with respect to the time scale ratio τ_x/τ_y. Parameters are the same as in Fig. 1(a), but with $P = 2, \tau_x = 0.02$. τ_y has been adjusted according to the ratio.

increases, it becomes increasingly more difficult to apply the phase space approach. We suggest this methodology to complement existing approaches, such as those mentioned in the Introduction [15,16], and we suggest that it can be particularly useful for abstract low-dimensional minimal models.

To make the present qualitative reconstruction more quantitative, we suggest local parameter fitting of the model output to clinical EEGs. Previous work has shown the application of such parameter fits to clinical data to determine a so-called "path through parameter space" [7,35]. Use of our minimal model in this context has the advantage that only local maxima are required for the fitting as the model can be preengineered qualitatively to the prototypic wave form and other relevant features. Also, optimization parameters and plausible parameter ranges can be suggested from the reverse-engineering process (see, e.g., Fig. 5).

Wave forms in clinical EEG are generally not exactly periodic and often irregular (cf. the recordings in Fig. 3). Such irregularity can be accounted for by the intrinsic noise of biological processes. In neural macroscopic models, intrinsic noise is modeled either by noisy inputs into the model equations [7,9,36] or generally by additive noise [31,37,38]. For a general additive noise term, we show in Appendix D (Fig. 9) the robustness of the minimal system with respect to certain regions and directions in phase space. Appendixes C and D show that the system is most sensitive to noisy inputs

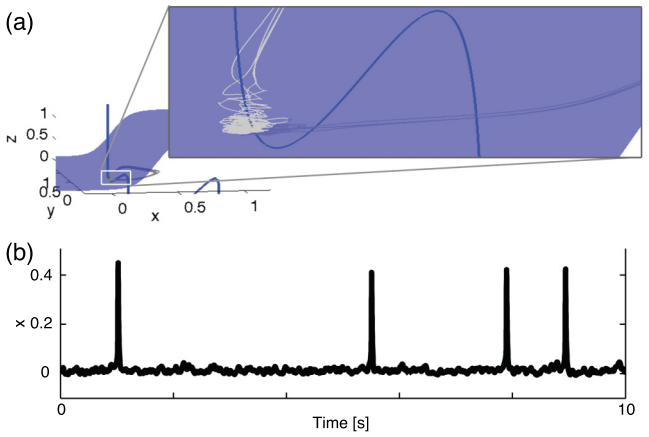

FIG. 7. (Color online) Phase space (a) and time course (b) of a noise-driven excitable fixed point. Refer to Fig. 2 for the plotting convention of the full phase space. The thin gray line in (a) is the time course of (b) plotted in the full phase space. The white box indicates the zoom region of the inset. The parameters are given in Appendix B. The 3D plot is in the Supplemental Material [28].

when it is close to bifurcation points (Fig. 10), or when it is in the presence of excitable (Fig. 7) or bistable structures (Fig. 8). This agrees with previous literature, where noise has been suggested as a key mechanism to induce epileptic activity by exploring bifurcations, or excitable or bistable phase space structures [17,34,36,39]. A potential way to test for the presence of both excitability and bistability in the brain is through active probing [8,40,41], for example, by testing the responses to repetitive photic or electric stimulation. This can help to better reconstruct the phase space and restrict the parameter ranges in the minimal model.

By reconstruction of dynamics in the minimal model, hypotheses are generated on either the mechanistic level (noise-driven activity, parameter-induced transitions) or on the parametric level (relative parameter changes, bifurcation types). To test the validity of these model-inferred hypotheses, one has to identify modeled excitatory and inhibitory processes with processes (or groups of processes) in physiologically

TABLE I. Parameters used for the figures. Connectivity parameters not listed have been set to zero. The parameters for the sigmoidal activation remain the same in all cases: $a = 1, \theta = 4$.

Figure	$C_{x,x}$	$C_{x,y}$	$C_{x,z}$	$C_{y,x}$	$C_{z,x}$	P	Q	R	τ_x	τ_y	τ_z
1(a),1(b)	24	− 20	0	40	0	1.5	− 2	0	0.013	0.013	0
1(c),1(d)	23	− 15	0	35	0	0.5	− 5	0	0.011	0.013	0
1(e),3(f)	25	− 15	0	35	0	− 1	− 5	0	0.01	0.013	0
1(g),1(h)	40	− 25	0	38	0	− 5	− 20	0	0.033	0.013	0
2	38	− 29	− 10	40	15	5	− 2	0	0.013	0.013	0.267
3(a),3(c)	24	− 20	− 15	40	7	3	− 2	0	0.013	0.013	0.267
3(d),3(f)	23	− 15	− 10	35	10	0.5	− 5	− 5	0.015	0.013	0.267
3(g),3(i)	23	− 15	− 10	35	10	3	− 5	− 5	0.015	0.013	0.267
3(j),3(l)	25	− 15	− 10	35	10	4	− 5	− 3	0.0225	0.03	0.12
4	38	− 29	− 10	40	20	3 to 5	− 2	0	0.013	0.013	0.267
5(d)	38	− 29	− 10	40	15 to 6	5	− 2	0	0.017	0.017	0.25
5(e)	38	− 29	− 10	40	15	5	− 2	0	0.017 to 0.036	0.017 to 0.036	0.25
7	35	− 30	− 10	40	15	− 0.5	− 5	0	0.013	0.013	0.267
8	40	− 25	− 10	38	15	− 2	− 20	− 10	0.033	0.013	0.067

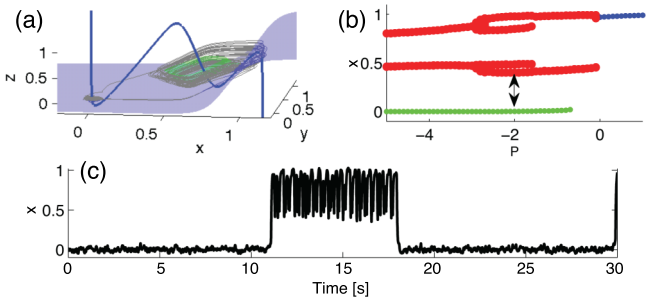

FIG. 8. (Color online) (a) Phase space with the trajectory of the time course in (c) shown in gray. Refer to Fig. 2 for the plotting convention of the full phase space. (b) Bifurcation diagram as a function of P in the full system. The double arrow marks the parameter used in (a) and (c). See Fig. 1 for the plotting convention. The 3D plot is in the Supplemental Material [28].

more detailed models, or directly with physiological processes in the brain.

When relating the minimal model to detailed biophysical models, different underlying correspondents might be lumped as one process in the minimal system. For example, the slow inhibitory process z could be referring to the regulation of extracellular potassium [42], glial processes in general [43], or subcortical input [44]. These processes have partly been included in physiologically more detailed models [36,45]. Therefore, in these models our hypotheses can be tested *in silico*.

For experimental testing, the variables of the minimal model need to be identified with corresponding neurophysiological observables. For instance, in the model we observe that, when a spike limit cycle is present, increasing the amount of fast inhibition of the excitatory variable E can abolish the limit cycle completely.[2] A simple model-generated hypothesis is therefore that ongoing epileptic spiking could be suppressed by a process that enhances fast inhibition. If fast inhibition is identified with $GABA_A$ inhibition of pyramidal neurons by interneurons, this would be consistent with experimental observations reported in Ref. [46], where the authors show that the presence of a $GABA_A$-enhancing antiepileptic drug (diazepam) suppresses ongoing spiking in a self-sustained status epilepticus in rats.

In general, such model-based hypothesis can first be tested in models that explicitly include the process of interest, e.g., drug action [47], and then confirmed in *in vitro* or *in vivo* neurophysiological experiments.

ACKNOWLEDGMENTS

We thank G. Wiegand, H. Muhle, M. Siniatchkin, U. Stephani (University of Kiel), and K. Schindler (Inselspital Bern), for discussion of clinical aspects of epilepsy and EEG data. We thank D. Garry, J. Pahle, and T. Biancalani for general discussion. We acknowledge financial support from BBSRC, EPSRC, and the University of Manchester.

APPENDIX A: EIGENVALUES OF THE SUBSYSTEM

The linear system

$$\begin{aligned}\frac{dx}{dt} &= -x + (C_{x,x}x + C_{x,y}y + P),\\ \frac{dy}{dt} &= -y + (C_{y,x}x + C_{y,y}y + Q)\end{aligned} \tag{A1}$$

has one fixed point at

$$x = \frac{\frac{P(C_{y,y}-1)}{C_{x,y}C_{y,x}} - \frac{Q}{C_{y,x}}}{1 - \frac{(C_{x,x}-1)(C_{y,y}-1)}{C_{x,y}C_{y,x}}}, \quad y = \frac{\frac{Q(C_{x,x}-1)}{C_{x,y}C_{y,x}} - \frac{P}{C_{x,y}}}{1 - \frac{(C_{x,x}-1)(C_{y,y}-1)}{C_{x,y}C_{y,x}}},$$

and its stability depends on the eigenvalues of the Jacobian, which are given by

$$\lambda_{1,2} = \frac{(C_{x,x}-1)+(C_{y,y}-1)}{2} \pm \sqrt{\frac{[(C_{x,x}-1)+(C_{y,y}-1)]^2}{4} - (C_{x,x}-1)(C_{y,y}-1) + C_{x,y}C_{y,x}}. \tag{A2}$$

From this we derive that the minimal feedback structures supporting an unstable focus (the real part of the eigenvalues positive and the imaginary part nonzero) are self-excitation of the excitatory process and mutual activation of the excitatory and inhibitory processes: $C_{x,y} < 0, C_{y,x} > 0, C_{x,x} > 1, |\frac{(C_{x,x}-1)^2}{4} - (C_{x,x}-1)| < |C_{x,y}C_{y,x}|$ for $C_{y,y} = 0$ and for all P, Q, R.

The corresponding system with sigmoid activation can have a fixed point with similar properties as in the linear system, where the intermediate parts of the nullclines intersect. This becomes clear when one approximates the system with sigmoid activation by a system with piecewise linear activation, where the slope of the piecewise linear activation is the same as the slopes at the inflection point of the sigmoid. The approximate bifurcation structures and related properties like excitability are preserved in the piecewise-linear case.

The system with different time scales has the same fixed points as the corresponding system with identical time scale parameters. However, the choice of time constants can have a strong influence on the existence of the limit cycle. The eigenvalues of the unstable focus (around which the limit cycle can exist) for the piecewise-linear system are

[2] When a spike limit cycle is present, increasing $C_{x,y}$ changes the shape of the x nullcline to be less steep, and hence the spike limit cycle can be realized only for higher values of P, or the spike limit cycle is completely abolished for all P.

given by

$$\lambda_{1,2} = \frac{\frac{(mC_{x,x}-1)}{\tau_x} + \frac{(mC_{y,y}-1)}{\tau_y}}{2} \pm \sqrt{\frac{\left(\frac{(mC_{x,x}-1)}{\tau_x} + \frac{(mC_{y,y}-1)}{\tau_y}\right)^2}{4} - \frac{(mC_{x,x}-1)}{\tau_x}\frac{(mC_{y,y}-1)}{\tau_y} + \frac{m^2 C_{x,y}C_{y,x}}{\tau_x\tau_y}}$$
$$= \frac{\frac{(mC_{x,x}-1)}{\tau_x} + \frac{(mC_{y,y}-1)}{\tau_y}}{2} \pm \sqrt{\frac{1}{\tau_x\tau_y}\left(\frac{\tau_y}{4\tau_x}(mC_{x,x}-1)^2 + \frac{\tau_x}{4\tau_y}(mC_{y,y}-1)^2 + 0.5(mC_{x,x}-1)(mC_{y,y}-1) + (m^2 C_{x,y}C_{y,x})\right)}. \quad \text{(A3)}$$

Here m is the slope of the piecewise-linear activation function (similar to a in the sigmoidal activation). This equation shows that for $C_{y,y} = 0$ and $C_{x,x} > 0$, increase of the ratios τ_x/τ_y and $\frac{1}{\tau_x\tau_y}$ increases the frequency of the unstable focus. Scans of τ_x/τ_y in the sigmoidal system confirm that the frequency increases and the amplitude decreases with increase of the ratio (see, for example, Fig. 6).

From Eq. (A3) it becomes apparent that the time scale ratio changes the Hopf bifurcation point. With the influence on the amplitude of the limit cycle the homoclinic and saddle-node on invariant circle bifurcation points will also be influenced by the time scale ratio.

APPENDIX B: PARAMETER TABLE

The parameters used in the figures are given in Table I.

APPENDIX C: EXCITABILITY AND BISTABILITY

The following two examples illustrate how epileptiform excitable and bistable phase space structures can be reconstructed. Type I and type II excitability can be found in the subsystem near the homoclinic bifurcation and the Hopf bifurcation, respectively. For valid time scale separation, these properties also exist in the full system. The nullcline plane intersects the lower fixed point manifold near the

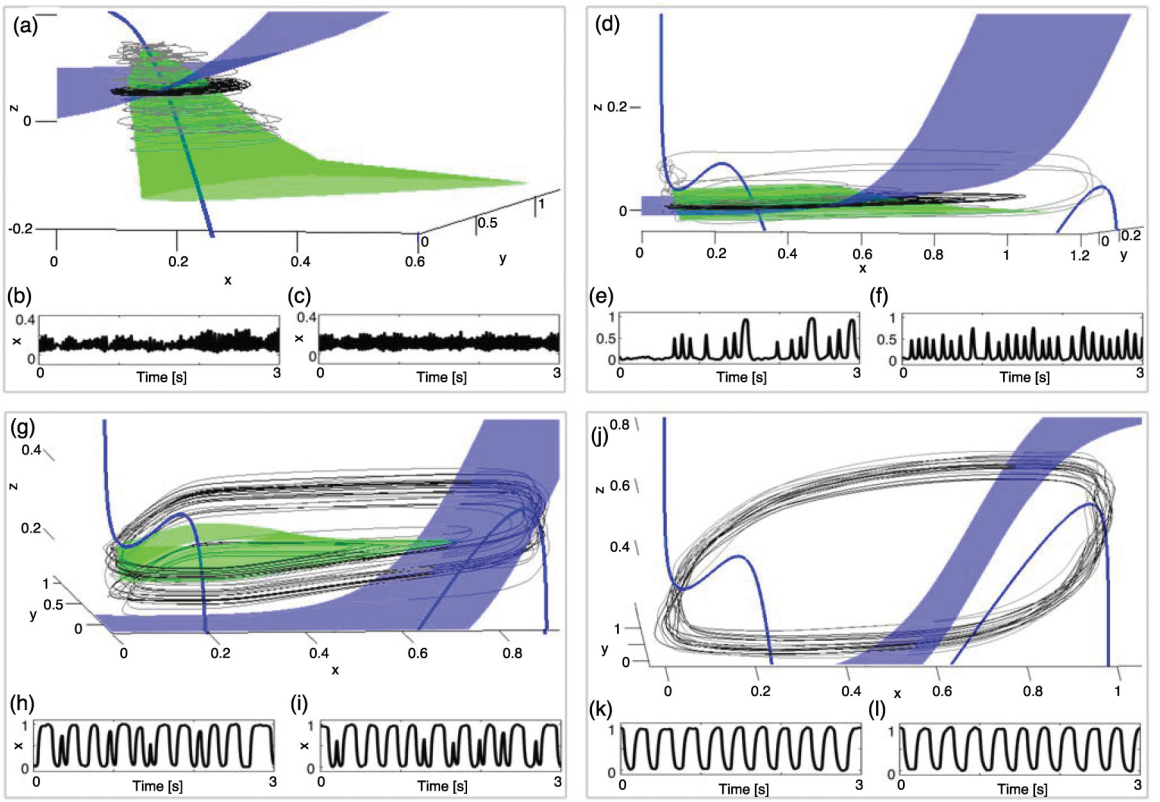

FIG. 9. (Color online) Prototypical attractors with scaled (black line) and unscaled (gray line) additive noise shown in phase space (a),(d),(g),(j). Time series of x of the corresponding prototype with scaled (c),(f),(i),(l) and unscaled (b),(e),(h),(k) additive noise. The parameters are as in Fig. 3. The 3D plots are in the Supplemental Material [28].

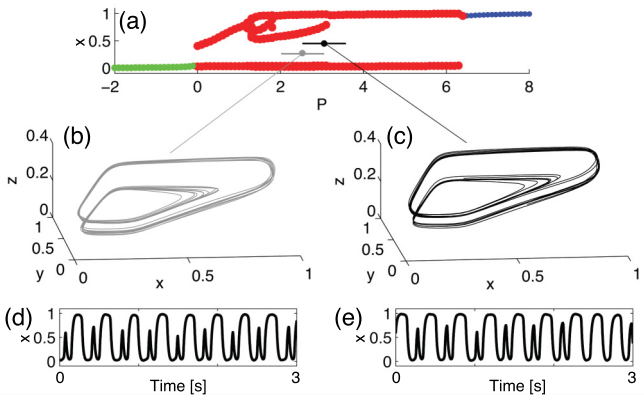

FIG. 10. (Color online) (a) Bifurcation scan for P of the full system without noise (plotting convention as in Fig. 1). The values for P used for (b) and (c) are indicated by the gray and black dot, respectively. The bars through the dots show the maximal noise amplitudes. (b),(c) Spike-wave attractors for different mean noise values of P in the full phase space. (d),(e) Time series corresponding to phase space plots in (b) and (c). The parameters are as in Fig. 3(g).

homoclinic bifurcation of the subsystem [see Fig. 7(a)]. When the system is perturbed over the separating manifold of the saddle, the trajectory has to rotate around the focus to return to the lower fixed point (type I excitability). The transient resembles an interictal spike. When the full system is in the stable fixed point which shows this "spike excitability," small perturbations [an additive noise term appended to Eq. (1)] can be used to reconstruct time series with irregular individual spikes (Fig. 7).

Figure 8 is an example of a system that is bistable between a fixed point and a spike-wave attractor as suggested for absence seizures by Ref. [17]. To achieve this, the spike-wave attractor (see Sec. III B) is used, and the position of the lower saddle-node manifold is modified such that it intersects the nullcline plane at the lower part [see Fig. 1(h) for the subsystem configuration]. The intermediate part of the nullcline plane separates the upper node from the limit cycle, as before, to form the stable spike-wave attractor [see Fig. 8(a)]. Figure 8(b) shows the bifurcation diagram of the full system for P. The bistable region between the lower fixed point and the spike-wave attractor can be seen. In this region, the addition of noise can result in irregular transitions between the two coexisting attractors [Fig. 8(c)].

APPENDIX D: THE SYSTEM UNDER NOISE PERTURBATION

To study the stability of prototypical attractors under added noise we consider Eq. (1) with an additive noise term.[3] Figure 9 shows simulations of each of the epileptic prototypes (Fig. 3) under unweighted (the noise term in all variables weighted by the same constant) and weighted noise perturbation (the noise term in all variables is weighted additionally by $\frac{\tau_x}{\tau_i}$, $i = x, y, z$).

While the attractors of the prototypes are robust to addition of noise in the x, y dimension, they are sensitive to noise in the z dimension when identical levels of noise are employed [see Figs. 9(b), 9(e), 9(h), and 9(k)]. The reason is that a change in the z direction translates to a big change in terms of fast local dynamics. When, however, the noise level is scaled relative to the corresponding time scale, the prototypes are robust against additive noise up to a certain noise level. This threshold noise level differs for the prototypes and depends on how close the attractors are to separating manifolds in phase space.

Furthermore, we study the effect of injected noise using the input parameters P, Q, or R as noisy parameters with a mean value at the same original constant value. In this case, the system will not be very sensitive to this kind of injected noise, as long as the noise does not induce the system to cross bifurcation points in the respective parameter [Figs. 10(b) and 10(d)]. This is in agreement with previous work, for example, [48]. If, however, the system is near a bifurcation point in either P, Q, or R, noise will induce a transition between the two types of behavior [Figs. 10(c) and 10(e)]. This is illustrated in Fig. 10 for the spike-wave prototype, where the same level of noise has been injected for P in the middle of the spike-wave region and at the bifurcation boundary to the wave limit cycle. Interestingly, the results are consistent with the occasional clinical observation of fragmented and irregular spike-wave sequences in addition to regular ones [49].

[3]To simulate the systems with noise in Appendixes C and D, different methods were used, including the Euler-Maruyama stochastic differential equation solver and fixed step ODE solvers. For the solvers, different step sizes, all significantly less than the noise discretization time step, were used to validate the results. Furthermore, different types of noise (normal and uniform) with different discretization time steps were simulated. All simulations using all methods agreed on the aspects of the results presented.

[1] E. Niedermeyer, *The Generalized Epilepsies: A Clinical Electroencephalographic Study* (Charles C. Thomas, Springfield, IL, 1972).
[2] W. Blume, G. Bryan Young, and J. Lemieux, Electroencephalogr. Clin. Neurophysiol. **57**, 295 (1984).
[3] *Niedermeyer's Electroencephalography: Basic Principles, Clinical Applications, and Related Fields*, 6th ed., edited by D. L. Schomer and F. L. da Silva (Lippincott Williams and Wilkins, Philadelphia, PA, 2011).
[4] J. Ziburkus, J. R. Cressman, E. Barreto, and S. J. Schiff, J. Neurophysiol. **95**, 3948 (2006).
[5] P. Suffczynski, F. Wendling, J.-J. Bellanger, and F. Da Silva, Proc. IEEE **94**, 784 (2006).
[6] G. Deco, V. Jirsa, P. Robinson, M. Breakspear, and K. Friston, PLoS Comput. Biol. **4**, e1000092 (2008).
[7] F. Wendling, F. Bartolomei, J. Bellanger, and P. Chauvel, Eur. J. Neurosci. **15**, 1499 (2002).
[8] F. H. Lopes da Silva, W. Blanes, S. N. Kalitzin, J. Parra, P. Suffczynski, and D. N. Velis, IEEE Trans. Biomed. Eng. **50**, 540 (2003).
[9] M. Breakspear, J. Roberts, J. R. Terry, S. Rodrigues, N. Mahant, and P. Robinson, Cereb. Cortex **16**, 1296 (2006).

[10] S. Rodrigues, J. R. Terry, and M. Breakspear, Phys. Lett. A **355**, 352 (2006).
[11] B. Molaee-Ardekani, P. Benquet, F. Bartolomei, and F. Wendling, NeuroImage **52**, 1109 (2010).
[12] M. Goodfellow, K. Schindler, and G. Baier, NeuroImage **55**, 920 (2011).
[13] M. Goodfellow, K. Schindler, and G. Baier, NeuroImage **59**, 2644 (2012).
[14] P. N. Taylor and G. Baier, J. Comput. Neurosci. **31**, 679 (2011).
[15] E. Marder and A. L. Taylor, Nat. Neurosci. **14**, 133 (2011).
[16] F. Frascoli, L. van Veen, I. Bojak, and D. T. Liley, Physica D **240**, 949 (2011).
[17] F. Da Silva, W. Blanes, S. Kalitzin, J. Parra, P. Suffczynski, and D. Velis, Epilepsia **44**, 72 (2003).
[18] M. Desroches, J. Guckenheimer, B. Krauskopf, C. Kuehn, H. Osinga, and M. Wechselberger, SIAM Rev. **54**, 211 (2012).
[19] E. Izhikevich, Int. J. Bifurcation Chaos Appl. Sci. Eng. **10**, 1171 (2000).
[20] J. Touboul, F. Wendling, P. Chauvel, and O. Faugeras, Neural Comput. **23**, 3232 (2011).
[21] H. Wilson and J. Cowan, Biophys. J. **12**, 1 (1972).
[22] S. Amari, Biol. Cybern. **27**, 77 (1977).
[23] H. Sakaguchi, Prog. Theor. Phys. **79**, 1061 (1988).
[24] R. Borisyuk and A. Kirillov, Biol. Cybern. **66**, 319 (1992).
[25] L. Monteiro, M. Bussab, and J. C. Berlinck, J. Theor. Biol. **219**, 83 (2002).
[26] A. Destexhe, J. Neurosci. **18**, 9099 (1998).
[27] N. Fenichel, J. Differ. Eq. **31**, 53 (1979).
[28] See Supplemental Material at http://link.aps.org/supplemental/10.1103/PhysRevE.85.061918 for 3D MATLAB figures of the phase space in Figs. 2, 3(a), 3(d), 3(g), 3(j), 4(b), 4(c), 5(b), 5(c), 7(a), 8(a), 9(a), 9(d), 9(g), and 9(j).
[29] H. Doose, *Das EEG bei Epilepsien im Kindes- und Jugendalter* (Desitin Arzneimittel, Hamburg, 2002).
[30] C. Panayiotopoulos, T. Obeid, and G. Waheed, Brain **112**, 1039 (1989).
[31] E. Wallace, M. Benayoun, W. van Drongelen, and J. D. Cowan, PLoS One **6**, e14804 (2011).
[32] M. C. Mackey and J. G. Milton, Ann. NY Acad. Sci. **504**, 16 (1987).
[33] F. Wendling, A. Hernandez, J. J. Bellanger, P. Chauvel, and F. Bartolomei, J. Clin. Neurophysiol. **22**, 343 (2005).
[34] P. Suffczynski, F. Lopes da Silva, J. Parra, D. Velis, and S. Kalitzin, J. Clin. Neurophysiol. **22**, 288 (2005).
[35] A. J. Nevado-Holgado, F. Marten, M. P. Richardson, and J. R. Terry, NeuroImage **59**, 2374 (2012).
[36] F. Marten, S. Rodrigues, P. Suffczynski, M. P. Richardson, and J. R. Terry, Phys. Rev. E **79**, 021911 (2009).
[37] G. Deco, V. Jirsa, A. R. McIntosh, O. Sporns, and R. Kotter, Proc. Natl. Acad. Sci. USA **106**, 10302 (2009).
[38] P. C. Bressloff, Phys. Rev. E **82**, 051903 (2010).
[39] F. Wendling, J. Bellanger, F. Bartolomei, and P. Chauvel, Biol. Cybern. **83**, 367 (2000).
[40] S. Kalitzin, D. Velis, and F. Lopes da Silva, Epilepsy Behav. **17**, 310 (2010).
[41] O. David, J. Bastin, S. Chabardès, L. Minotti, and P. Kahane, Front. Syst. Neurosci. **4**, 148 (2010).
[42] F. Fröhlich, M. Bazhenov, V. Iragui-Madoz, and T. J. Sejnowski, Neuroscientist **14**, 422 (2008).
[43] C. Steinhäuser and G. Seifert, Eur. J. Pharmacol. **447**, 227 (2002).
[44] A. D. Norden and H. Blumenfeld, Epilepsy Behav. **3**, 219 (2002).
[45] R. C. Sotero and R. Martinez-Cancino, Neural Comput. **22**, 969 (2010).
[46] A. M. Mazarati, R. A. Baldwin, R. Sankar, and C. G. Wasterlain, Brain Res. **814**, 179 (1998).
[47] B. M. Bouwman, P. Suffczynski, F. H. Lopes da Silva, E. Maris, and C. M. van Rijn, Eur. J. Neurosci. **25**, 2783 (2007).
[48] A. Hutt, in *Modeling Phase Transitions in the Brain*, Springer Series in Computational Neuroscience, Vol. 4 (Springer, New York, 2010), pp. 53–80.
[49] L. G. Sadleir, K. Farrell, S. Smith, M. B. Connolly, and I. E. Scheffer, Neurology **67**, 413 (2006).